

X-ray absorption of cold gas: Simulating interstellar molecular clouds in the laboratoryI. Gissis^{ⓧ,*}, A. Fisher,[†] and E. Behar^{ⓧ,‡}*Physics Department, Technion, Israel Institute of Technology, Haifa 3200003, Israel*

(Received 19 March 2021; accepted 23 June 2021; published 13 July 2021)

Galactic and extragalactic sources produce x-rays that are often absorbed by molecules and atoms in giant molecular clouds (GMCs), which provides valuable information about their composition and physical state. We mimic this phenomenon with a laboratory Z-pinch x-ray source, which is impinged on neutral molecular gas. This technique produces a soft x-ray pseudocontinuum using a pulsed-current generator. The absorbing gas is injected from a 1-cm-long planar gas-puff without any window or vessel along the line of sight. An x-ray spectrometer with a resolving power of $\lambda/\Delta\lambda \sim 420$, comparable to that of astrophysical space instruments, records the absorbed spectra. This resolution clearly resolves the molecular lines from the atomic lines, thus motivating the search for a molecular signature in astrophysical x-ray spectra. The experimental setup enables different gas compositions and column densities. *K*-shell spectra of CO₂, N₂, and O₂ reveal a plethora of absorption lines and photoelectric edges measured at molecular column densities between $\sim 10^{16}$ and 10^{18} cm⁻² typical of GMCs. We find that the population of excited states, contributing to the edge, increases with gas density.

DOI: [10.1103/PhysRevE.104.015205](https://doi.org/10.1103/PhysRevE.104.015205)**I. INTRODUCTION**

X-rays from x-ray binaries (XRBs) and active galactic nuclei (AGNs) are often absorbed in interstellar (ISM) and intergalactic (IGM) media. Giant molecular clouds (GMCs) are abundant in the ISM and in star-forming regions. One of the main questions relevant to GMCs involves their chemistry and heating mechanism affected by x-rays, shock-waves, and cosmic rays [1]. In x-ray dominated regions (XDRs), the x-rays penetrate deep into the cloud, releasing secondary electrons, which heat, dissociate, and further ionize the gas. IR and mm emission of molecular tracers provide temperature and composition diagnostics [2,3] including for high redshift AGNs [4]. Complementary diagnostics comes from high-resolution x-ray (0.3–10 keV) absorption [5] and fluorescence [6]. Thus, it is important to study the x-ray absorption of these tracers in the laboratory.

Laboratory molecular absorption

Near-edge x-ray absorption fine structure (NEXAFS) is a common method to characterize the elemental composition of thin solid samples by probing the fine absorption features near the photoelectric edge. NEXAFS is originally and routinely performed in large beam facilities, i.e., synchrotrons [7] or free-electron lasers [8]. It is of high interest to various scientific disciplines such as the study of organic sheets [9], nanoscale samples [10], inorganic polymers [11], and astrophysical dust [12,13]. Table-top NEXAFS systems that

can carry out a large volume of tests at a high repetition rate are therefore desirable. Laser produced plasma (LPP) is the leading technique [14]. However, table-top LPPs require hundreds of shots to obtain a single high signal-to-noise ratio (SNR) spectrum. We have developed the GLIDER [15], a compact pulsed-power x-ray source of $\sim 10^{17}$ erg s⁻¹, which enables the measurement of NEXAFS of any matter-phase in an individual ~ 10 ns shot and dozens of shots per hour. In this paper, we report on NEXAFS diagnostics of astrophysical molecules found in GMCs.

II. EXPERIMENTAL SETUP AND METHODOLOGY

The experimental setup is depicted in Fig. 1. A gas-puff Z-pinch plasma x-ray source is produced using the GLIDER generator [15]. The Z-pinch source is optimized for absorption measurements of the CNO *K*-shell spectral range (20–50 Å) by using imploding Kr gas. Unlike low-*Z* elements, Kr has a multitude of blended *M*-shell lines that produce a pseudo-continuum soft x-ray and UV back-lighter to be absorbed by the CNO gas. The absorbing gas is injected through a second gas-puff along the line of sight, ~ 300 mm away from the pinch, and decoupled from it. The gas-puff injector is fast enough to prevent interaction between the absorber and the source. A reflection grating spectrometer (RGS) combined with a gated microchannel plate (MCP) detector records the absorption spectrum. Importantly, we avoid polymers such as polyimide or mylar windows because they are comprised of C, N, and O, which absorb strongly in the spectral range of interest. Indeed, our high-resolution spectra of polyimide revealed significant C NEXAFS features. To avoid ambiguous diagnostics and to still protect the grating from debris and stray light, a glass capillary array is placed between the gas absorber and the grating entrance slit.

*itaigiss@gmail.com

†amnon.fisher@gmail.com

‡behar@physics.technion.ac.il

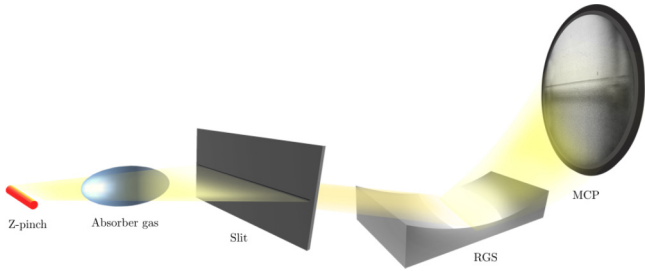


FIG. 1. Schematic experimental setup.

A. Wavelength calibration

Wavelength calibration was achieved using accurately known emission lines of highly ionized K -shell C, N, and O in dedicated Z-pinch shots with no absorber. To calibrate the O K -edge around 23 Å, the resonance lines of $N^{+5,+6}$ and $O^{+6,+7}$ are used. To calibrate the N K -edge around 31 Å, the resonant lines of $C^{+4,+5}$ and $N^{+5,+6}$ are used. The C K -edge around the 42 Å region was calibrated using both first-order diffraction C lines, e.g., at 33.736 (Ly α), 40.2678 (He α), 34.973 (He β), and second-order O lines, e.g., at 37.9340 (Ly α) and 43.202 (He α). Each ~ 10 Å range is calibrated using 5–10 peaks resulting in a systematic wavelength uncertainty of ≤ 7 mÅ. The spectrometer alignment is sensitive to temperature fluctuations. Therefore, spectral calibration was performed within minutes before or after the absorption shots.

B. Transmission spectral modeling

Transmission spectra are obtained by dividing an absorbed spectrum by one in a separate shot, which is unabsorbed in the range of interest. The transmission is defined as $e^{-\tau}$, where τ is the optical depth. The column density N of the absorber is related to the optical depth through $\tau = N\sigma$, where $\sigma(\lambda)$ is the cross-section profile for absorption in a spectral line or an edge. Column densities are estimated by dividing the measured $\tau(\lambda)$ by the published $\sigma(\lambda)$ [16]. The column density

is also $N = \int n(l) dl$, where $n(l)$ is the number density along the line of sight and is measured independently, as described in Sec. III B.

Each NEXAFS is modeled with a single edge and several resolved lines. The edge is modeled with a λ^3 profile (hydrogenic approximation) and the lines are modeled as Gaussians with fitted widths. Since we did not observe ionized or highly excited states, we assume all molecules are in their electronic ground state, but they could be vibrationally or rotationally excited. These excitations may be reflected in the absorption lines, but the edge still manifests the total molecular column density. The entire model was further convoluted with a Gaussian of $\sigma = 50$ –70 m Å accounting for the instrumental broadening. The data are fitted using NASA's Xspec spectral analysis code [17].

III. RESULTS

In Fig. 2 we present normalized NEXAFS spectra of CO_2 , N_2 , and O_2 . The models capture all main features identified in the literature to within ~ 1 eV. The results are summarized in Tables I, II, and III. The molecular neutral $K\alpha$ and the edge are clearly resolved in all three spectra. No ionized spectral lines are found short-ward of the edge. In C and N the neutral atom $K\alpha$ is resolved and is ~ 10 times weaker than the molecular $K\alpha$. Hence, the molecules are essentially neutral and only mildly dissociated.

A few exceptional details are worth noting: The molecular $K\alpha$ in all CO_2 shots is split into two peaks (nos. 2 and 3 in Fig. 2). The mean peak value is 42.63 Å, consistent with the $(2\sigma_g)^{-1}2\pi\mu$ transition (see Ref. [16], Fig. 4.2.5). The deep feature at 39.8 Å (no. 9) dominates the edge as it does in [18]. The edge starts at 41.84 Å and its recovery begins below 39 Å.

In N_2 as well, almost all the absorption features fit their tabulated positions to within ~ 1 eV. An exception is the edge, which is measured here ~ 3 eV above the value in [16]. This is likely due to blending of the edge with the strong double-excitation feature at ~ 413 eV (see Ref. [16], Fig. 3.2.6).

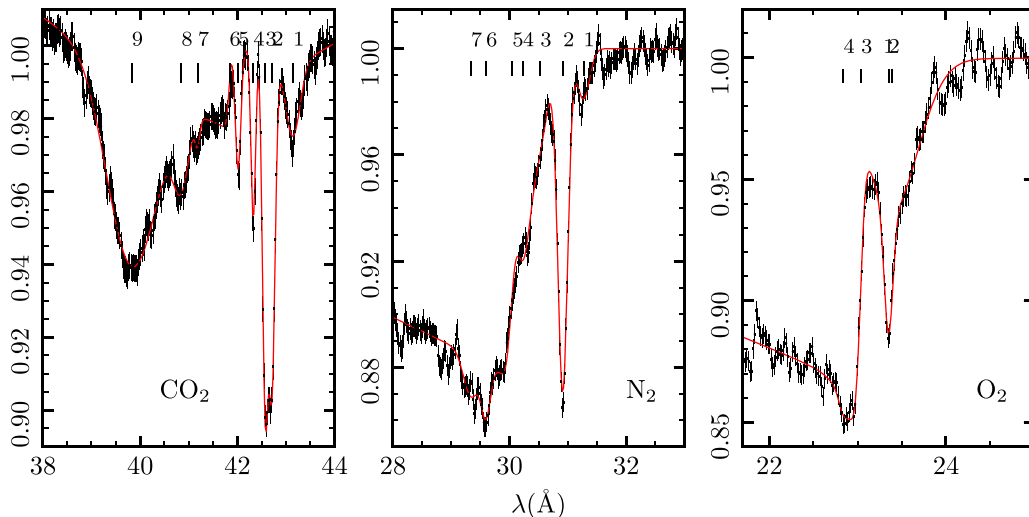


FIG. 2. Transmission spectra of CO_2 (C edge), N_2 , and O_2 over a Kr back-lighter. The best-fit model is plotted in solid red. The resolved transitions are marked on the figure and detailed in Tables I, II, and III.

TABLE I. CO₂ absorption lines and photoelectric edge around the C *K*-edge and their 1σ confidence interval.

No.	Central wavelength (Å)	Central energy (eV)	Literature (eV)	Assignment
1	43.15 ^{+0.02} _{-0.01}	287.4 ^{+0.1} _{-0.3}	285 ^a	1s2s ² 2p
2	42.72 ^{+0.02} _{-0.01}	290.3 ^{+0.1} _{-0.3}	290.77 ^b	(2σ _g) ⁻¹ 2π _u
3	42.58 ^{+0.02} _{-0.01}	291.3 ^{+0.1} _{-0.1}		
4	42.33 ^{+0.02} _{-0.01}	293.0 ^{+0.1} _{-0.1}	292.74 ^b	(2σ _g) ⁻¹ 5σ _g
5	42.02 ^{+0.01} _{-0.01}	295.1 ^{+0.1} _{-0.1}	295 ^c	3p
6	41.84 ^{+0.01} _{-0.02}	296.4 ^{+0.1} _{-0.1}	297.6 ^c	IP
7	41.19 ^{+0.01} _{-0.02}	301.1 ^{+0.1} _{-0.1}	300.5–301 ^c	shake-up
8	40.85 ^{+0.01} _{-0.04}	303.6 ^{+0.2} _{-0.1}	304.2 ^c	shake-up
9	39.83 ^{+0.01} _{-0.04}	311.4 ^{+0.2} _{-0.1}	311–314 ^{b,c}	shake-up ^d

^aReference [19]—mean value for all transitions.

^bReference [16].

^cReference [18].

^dBlended with σ* shape-resonance.

In O₂ the *K*α resonance comprises a few transitions. We fit it with two blended peaks at 23.37 Å, a broad one (no. 1 in Fig. 2) and a narrow one (no. 2). Unlike N₂ and CO₂, in O₂ the atomic O *K*α at ~527 eV [22] is absent and likely obscured by the broad no. 1 feature. Our confidence in the O₂ interpretation is lower than in N₂ or CO₂ because the Kr emission in this energy range is not as smooth, and residual Kr emission may linger in the transmission spectrum.

A. Column density measurements

For the sample spectra of Fig. 2 we obtained 1.2 ± 0.1, 10 ± 2, 11 ± 2 in units of 10¹⁶ cm⁻² for the CNO edges. This 10–20 % uncertainty is attributed to the fitting process of the σ(λ) profile to the measured τ(λ).

A significant advantage of our experiment is the flexibility to control the absorber density and therefore the column density. In Fig. 3 we present a set of experiments with N₂ at different initial plenum pressures. It can be seen from the figure that all NEXAFS features deepen as the pressure (and density) is increased.

TABLE II. Measured N₂ absorption lines and photoelectric edge and their 1σ confidence interval.

No.	λ (Å)	E (eV)	Literature (eV)	Assignment
1	31.27 ^{+0.02} _{-0.01}	396.6 ^{+0.2} _{-0.3}	396 ^a	1s
2	30.92 ^{+0.02} _{-0.01}	401.1 ^{+0.2} _{-0.2}	400.96 ^b	2pπ _g (π*)
3	30.53 ^{+0.02} _{-0.02}	406.2 ^{+0.2} _{-0.2}	406.13 ^b	3sσ _g
4	30.23 ^{+0.01} _{-0.02}	410.3 ^{+0.2} _{-0.2}	408.36 ^b	4sσ _g /3d
5	30.05 ^{+0.01} _{-0.02}	412.8 ^{+0.2} _{-0.2}	413 ^c	Double excitation
			409.9 ^c	IP
6	29.60 ^{+0.01} _{-0.02}	419.0 ^{+0.2} _{-0.2}	418.9 ^b	σ _u , <i>l</i> = 3
7	29.34 ^{+0.01} _{-0.02}	422.7 ^{+0.3} _{-0.2}	421 ^b	shake-up

^aReference [20].

^bReference [21].

^cReference [16].

TABLE III. O₂ absorption lines and photoelectric edge and their 1σ confidence interval.

No.	λ (Å)	E (eV)	Literature (eV)	Assignment
1	23.39 ^{+0.02} _{-0.01}	530.3 ^{+0.2} _{-0.5}	530.8 ^a	π*
2	23.35 ^{+0.02} _{-0.01}	531.0 ^{+0.2} _{-0.2}		
3	23.04 ^{+0.01} _{-0.01}	538.3 ^{+0.3} _{-0.2}	~540.5 ^b	IP
4	22.84 ^{+0.01} _{-0.03}	543.0 ^{+0.4} _{-0.2}	539.3 ^b	σ*

^aReference [21]. Lines 1 and 2 are blended, while line 1 is broadened (Fig. 2).

^bReference [16]. We measure a broad σ* shape-resonance, next to the edge.

The measured N₂ column densities are presented in Fig. 4 as a function of the pressure, separately for the *K*α resonance (blue diamonds) and the edge (red circles). The values deduced from the edge are consistently higher than those deduced by the line. This ratio gradually increases with the plenum pressure. The N₂ edge cross-section is enhanced by additional features of excited molecules (see Ref. [16], Fig. 3.2.6). This increases the opacity at the edge and thus the deduced column density by more than a factor of 2. The remaining discrepancy between the edge and the line column density could be explained by the lines being absorbed only by ground-state molecules, while the edge is produced also by excited molecules in the ground configuration, and this excitation increases with pressure. Supporting evidence is the strong shake-up features measured in both CO₂ and N₂ (see

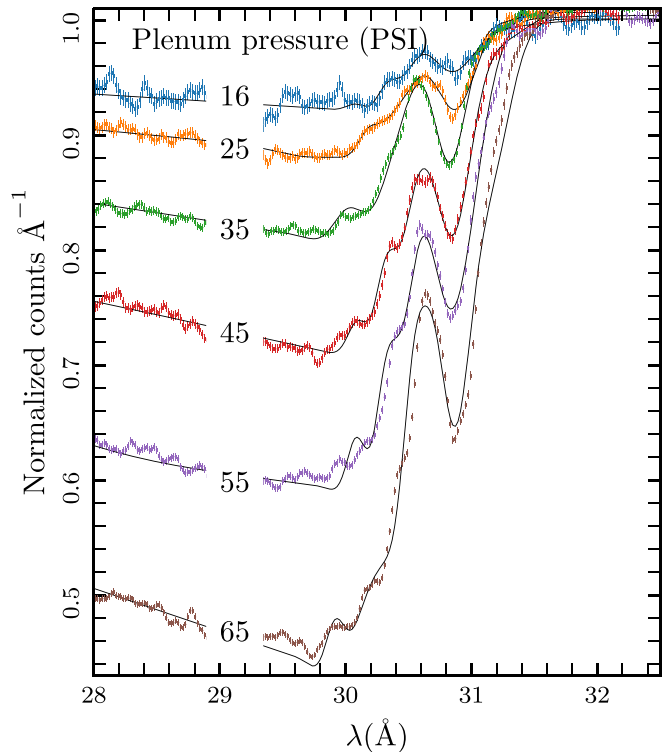


FIG. 3. Spectra of N₂ absorber on a Kr pinch background. The absorber puff plenum pressure in each shot is written on its corresponding spectrum.

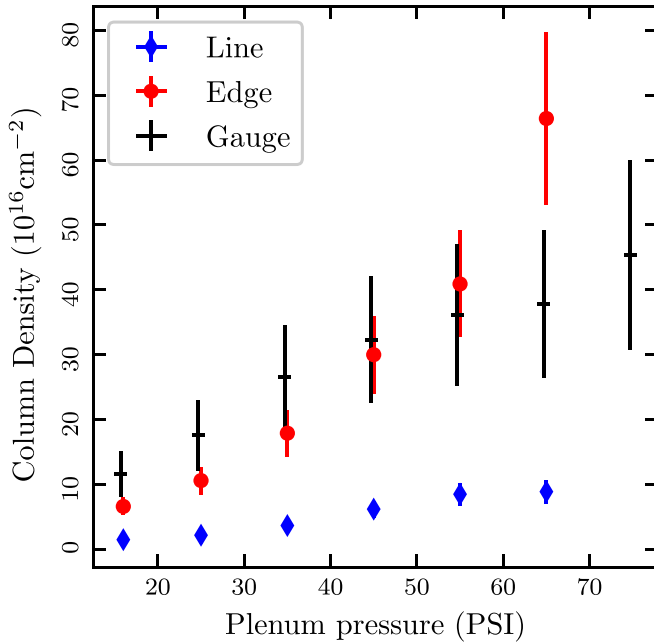


FIG. 4. Column density as a function of the absorber puff plenum pressure. Measurements are based on the line, edge, and a piezoelectric pressure gauge. The column density uncertainties reflect also the variance between shots.

Tables I and II) following the x-ray and UV excitation, which requires a broadband source similar to astrophysical sources.

The lack of significant heating and dissociation resembles less an XDR and more a remote GMC. This may be due to the relatively short x-ray pulse of ~ 10 ns, compared to the long dissociation times of $\sim \mu\text{s}$. The preceding UV pulse is also short, ~ 30 ns. The dissociation time $t_{\text{diss}} = (F\sigma)^{-1}$, where $F = 10^{23}$ ph s⁻¹ cm⁻² is the measured photon flux above 10 eV [15]. The cross-section is $\sigma = 10^{-18}$ – 10^{-16} cm² varying over the spectral band [23], which results in $t_{\text{diss}} = 0.1$ – 10 μs .

B. Independent density measurement

The pressure of the absorber was measured independently with a piezoelectric gauge, located downstream from the absorber puff nozzle exit, at the vertical position of the spectrometer slit. The gauge measures the stagnation pressure, which has a fixed ratio to the isentropic pressure and to the number density. The column density is this number density times the known planar nozzle length of 1 cm. The de-

duced gas column density is plotted in Fig. 4 as the black crosses. The agreement between the spectroscopically deduced column densities and the gauge measurement enhances our confidence in the cross-sections used, even though there are experimental uncertainties.

Beyond the 10–20 % uncertainty in the column density measured in an individual shot, the transmission spectra (Figs. 2 and 3) vary from shot to shot by $\sim 15\%$. These variations between shots stem from the imperfect mechanics of the absorber puff, and they are reflected in the error bars in Fig. 4. The gauge density uncertainty results from the statistical repeatability of the injected gas density and the gauge SNR. All sum up to 30% uncertainty.

IV. CONCLUSIONS

We present an experiment to measure x-ray absorption by gaseous abundant molecules and atoms, mimicking astrophysical absorption in the ISM. In this experiment, absorption of abundant astrophysical gases is measured with a pulsed-power x-ray source. We measured high-resolution NEXAFS spectra of CO₂, N₂, and O₂, identifying numerous absorption lines. In the present experiment, the gas is excited by a broadband pseudocontinuum Kr Z-pinch source. Therefore, the absorber is photoexcited similarly to molecular clouds exposed to x-ray astrophysical sources. We demonstrate a wide dynamic range of absorber densities. Utilizing the x-ray astronomy fitting code Xspec, we deduced column densities of $\sim 10^{17}$ cm⁻², in good agreement with independently measured pressure.

The present setup paves the way for many more high-resolution x-ray absorption experiments that can support spectral interpretation of astrophysical sources and materials science research. Improving the accuracy of the independent density measurement will allow us to benchmark excitation cross-sections. We are now preparing to integrate a second spectrometer and measure the absorbed and unabsorbed spectra simultaneously, thus improving the accuracy of the NEXAFS spectrum. We are currently extending our measurements to photoionized atomic species, also abundant in the ISM.

ACKNOWLEDGMENTS

We acknowledge support by the Center of Excellence of the ISF (Grant No. 2752/19), and a grant from the Pazy Foundation. We thank S. Bialy for useful comments on the manuscript.

- [1] R. Meijerink and M. Spaans, Diagnostics of irradiated gas in galaxy nuclei. I. A far-ultraviolet and X-ray dominated region code, *Astron. Astrophys.* **436**, 397 (2005).
- [2] A. G. G. M. Tielens, The molecular universe, *Rev. Mod. Phys.* **85**, 1021 (2013).
- [3] P. R. Maloney, D. J. Hollenbach, and A. G. G. M. Tielens, X-Ray-irradiated molecular gas. I. Physical processes and general results, *Astrophys. J.* **466**, 561 (1996).

- [4] L. Vallini, A. Pallottini, A. Ferrara, S. Gallerani, E. Sobacchi, and C. Behrens, CO line emission from galaxies in the Epoch of Reionization, *Mon. Not. R. Astron. Soc.* **473**, 271 (2018).
- [5] K. Joachimi, E. Gattuzz, J. A. García, and T. R. Kallman, On the detectability of CO molecules in the interstellar medium via X-ray spectroscopy, *Mon. Not. R. Astron. Soc.* **461**, 352 (2016).

- [6] T. Kawamuro, T. Izumi, K. Onishi, M. Imanishi, D. D. Nguyen, and S. Baba, AGN x-ray irradiation of CO gas in NGC 2110 revealed by Chandra and ALMA, *Astrophys. J.* **895**, 135 (2020).
- [7] B. M. Kincaid and P. Eisenberger, Synchrotron Radiation Studies of the *k*-Edge Photoabsorption Spectra of Kr, Br₂, and GeCl₄: A Comparison of Theory and Experiment, *Phys. Rev. Lett.* **34**, 1361 (1975).
- [8] H. Iwayama, M. Nagasaka, I. Inoue, S. Owada, M. Yabashi, and J. R. Harries, Demonstration of transmission mode soft x-ray nexafs using third- and fifth-order harmonics of FEL radiation at SACLA BL1, *Appl. Sci.* **10**, 7852 (2020).
- [9] G. Hähner, Near edge x-ray absorption fine structure spectroscopy as a tool to probe electronic and structural properties of thin organic films and liquids, *Chem. Soc. Rev.* **35**, 1244 (2006).
- [10] T. Hemraj-Benny, S. Banerjee, S. Sambasivan, M. Balasubramanian, D. Fischer, G. Eres, A. Puretzky, D. Geohegan, D. Lowndes, W. Han, J. Misewich, and S. Wong, Near-edge x-ray absorption fine structure spectroscopy as a tool for investigating nanomaterials, *Small* **2**, 26 (2006).
- [11] O. Dhez, H. Ade, and S. Urquhart, Calibrated nexafs spectra of some common polymers, *J. Electron Spectrosc. Relat. Phenom.* **128**, 85 (2003).
- [12] E. Costantini, S. T. Zeegers, D. Rogantini, C. P. de Vries, A. G. G. M. Tielens, and L. B. F. M. Waters, X-ray extinction from interstellar dust. Prospects of observing carbon, sulfur, and other trace elements, *Astron. Astrophys.* **629**, A78 (2019).
- [13] J. C. Lee, J. Xiang, B. Ravel, J. Kortright, and K. Flanagan, Condensed matter astrophysics: A prescription for determining the species-specific composition and quantity of interstellar dust using x-rays, *Astrophys. J.* **702**, 970 (2009).
- [14] P. Wachulak, M. Duda, A. Bartnik, A. Sarzyński, Ł. Wegrzyński, M. Nowak, A. Jancarek, and H. Fiedorowicz, Compact system for near edge x-ray fine structure (nexafs) spectroscopy using a laser-plasma light source, *Opt. Express* **26**, 8260 (2018).
- [15] I. Gissis, E. Behar, A. Fisher, S. Aricha, E. Yeger, U. Avni, and I. Schnitzer, Glidera pulsed-current generator for laboratory astrophysics x-ray absorption experiments, *Rev. Sci. Instrum.* **91**, 024701 (2020).
- [16] J. Berkowitz, *Atomic and Molecular Photoabsorption: Absolute Partial Cross Sections* (Elsevier Science, Amsterdam, 2015).
- [17] K. A. Arnaud, *Astronomical data analysis software and systems V*, edited by G. H. Jacoby and J. Barnes, A.S.P. Conference Series Vol. 101 (Astronomical society of the Pacific, 1996).
- [18] T. K. Sham, B. X. Yang, J. Kirz, and J. S. Tse, K-edge near-edge x-ray-absorption fine structure of oxygen- and carbon-containing molecules in the gas phase, *Phys. Rev. A* **40**, 652 (1989).
- [19] M. F. Hasoglu, S. A. Abdel-Naby, T. W. Gorczyca, J. J. Drake, and B. M. McLaughlin, K-Shell photoabsorption studies of the carbon isonuclear sequence, *Astrophys. J.* **724**, 1296 (2010).
- [20] J. García, T. R. Kallman, M. Witthoef, E. Behar, C. Mendoza, P. Palmeri, P. Quinet, M. A. Bautista, and M. Klapisch, Nitrogen k-shell photoabsorption, *Astrophys. J., Suppl. Ser.* **185**, 477 (2009).
- [21] A. Hitchcock and C. Brion, K-shell excitation spectra of CO, N₂ and O₂, *J. Electron Spectrosc. Relat. Phenom.* **18**, 1 (1980).
- [22] B. M. McLaughlin, C. P. Ballance, K. P. Bowen, D. J. Gardenghi, and W. C. Stolte, High precision k-shell photoabsorption cross sections for atomic oxygen: Experiment and theory, *Astrophys. J.* **771**, L8 (2013).
- [23] W. Huebner and J. Mukherjee, Photoionization and photodissociation rates in solar and blackbody radiation fields, *Planet. Space Sci.* **106**, 11 (2015).